Composites Part B 185 (2020) 107793

Contents lists available at ScienceDirect

Composites Part B

journal homepage: www.elsevier.com/locate/compositesb

The CNT/PSt-EA/Kevlar composite with excellent ballistic performance

Saisai Cao, Haoming Pang, Chunyu Zhao, Shouhu Xuan **, Xinglong Gong *

CAS Key Laboratory of Mechanical Behavior and Design of Materials, Department of Modern Mechanics, CAS Center for Excellence in Complex System Mechanics, University of Science and Technology of China (USTC), Hefei, 230027, PR China

ARTICLE INFO

Keywords:
fabrics/textiles
Nano particles
Impact behavior
Finite element analysis (FEA)
Shear thickening fluid

ABSTRACT

This work reports a new type of ballistic composite which is prepared by integrating the carbon nanotube-polystyrene ethyl acrylate (CNT/PSt-EA) based shear thickening fluid (C-STF) with Kevlar fabric. Because the rheological property of the PSt-EA based STF is significantly enhanced by the CNT, the C-STF/Kevlar offers better ballistic property than Kevlar fabric. The ballistic test indicated that the ballistic limit velocity (v_{bl}) of Kevlar could be improved from 84.6 m/s to 96.5 m/s by impregnating the C-STF. Here, the optimum addition of CNT for C-STF/Kevlar is 1.0% and excessive CNT addition reduces the reinforcement effect. Besides, as the volume fraction of dispersed phase in STF increased from 53.5% to 58.5%, the v_{bl} increased from 92.9 m/s to 99.5 m/s. The fabric layer number also plays a critical role in the ballistic property of C-STF/Kevlar. By combining the finite element analysis (FEA) results of ballistic impact with the quasi-static puncture and yarn pull-out results, the enhanced anti-impact mechanism is obtained. It is found that the friction coefficient between the yarns is strengthened and the bearing area of the fabric is increased by doping STFs, thereby the ballistic performance of Kevlar is improved. This work achieves the regulation of ballistic performance of Kevlar composites.

1. Introduction

In the war, body armor plays an important role in reducing bullet damage and even saving soldiers' lives. To reduce the weight of the body armor and facilitate the movement of soldiers, high-strength fibers such as Kevlar, Twaron, etc. are used to manufacture soft body armor [1–3]. However, in order to meet the protection requirements, multi-layers are often required in body armor, thus the soft armor is very thick which reduces the wearing comfort [4,5]. Therefore, the high ballistic performance, well flexibility, and light weight are simultaneously concerned in developing high quality body armor.

Till 2003, the soft body armor prepared by incorporating shear thickening fluid (STF) into the Kevlar fabrics has attracted increasing interests. STF is a kind of dense granular suspension [6]. It exhibits the properties of Newtonian fluid at low shear rate. As the shear rate exceeds a critical value, the viscosity of STF increases dramatically. After removing the shear, it can recover to the initial state [7]. Due to this reversible shear thickening effect, the STF possesses broad application in the field of damping and protection [8–12]. After introducing the STF into the Kevlar, the STF/Kevlar exhibits high anti-impact property. The SiO_2 based STFs are widely applied in the field of fabric reinforcement [8,13]. However, the density of SiO_2 is large, and the Kevlar impregnated with STF (STF/Kevlar) has a lot of enhancement space. In recent years, a series of polymer-based STF have been reported [14,15]. Among them, a polystyrene ethyl acrylate (PSt-EA)-based STF has the characteristics of low density and strong shear thickening effect, which has great potential in improving the protective properties of fabrics [16,17].

The ballistic resistance performance of STF/Kevlar was firstly investigated by Lee et al. [18]. Since then, researchers have conducted extensive research on the protective properties of this kind of composites [19,20]. The mechanical properties of STF/Kevlar were investigated by many researchers [21–23]. Decker [24] and Xu [25] et al. focused on the low velocity impact and conducted the stab resistance test [26]. Park [27] and Tan [28] et al. employed the ballistic test to investigate its effectiveness on high velocity impact [29]. In these works, the yarn pull-out test was implemented to indicate the friction between fabric yarns [30,31]. These experimental results showed that the impregnation of STF had a significant enhancement to the protective effect of the fabric. A common qualitative interpretation was that the STF increased the friction between the yarns, increasing the load-bearing area of the fabric and thus enhancing the protective effect of the fabric. Meanwhile, the researchers also improved the protective property of the composite

* Corresponding author.
** Corresponding author.
E-mail addresses: xuansh@ustc.edu.cn (S. Xuan), gongxl@ustc.edu.cn (X. Gong).

https://doi.org/10.1016/j.compositesb.2020.107793
Received 6 June 2019; Received in revised form 5 December 2019; Accepted 18 January 2020
Available online 23 January 2020

Table 1
The definition and detailed data of the STF/Kevlar and C-STF/Kevlar composites.

Name	Impregnated STF			Average weight (g)		Weight addition (%)
	PSt-EA (vol. %)	EG (vol. %)	CNT (wt. %)	Before impregnation	After impregnation	
SN	0	0	0			0
SF1	53.5	46.5	0	2.460	2.968	21.1
SF2	56.0	44.0	0	2.456	2.890	18.3
SF3	58.5	41.5	0	2.479	2.915	18.3
SC1	53.5	46.5	1.0	2.466	2.958	20.7
SC2	53.5	46.5	1.5	2.466	3.023	23.3
SE	0	100	0	2.443	2.695	11.1

by adding a reinforcing agent to the STF such as carbon nanotube (CNT) [31,32], SiC [33,34] and so on. The additions improved the rheological behavior of STF and then enhanced the protective properties of composites.

Although the experimental methods can characterize the protective effect of STF/Kevlar composite, it is not conducive to analyzing the mechanical details. The finite element analysis (FEA) is a good complement to the experiment. On the one hand, many detailed mechanical characteristics that cannot be obtained by experiments are available for FEA. On the other hand, the behavior of materials can be predicted by FEA more conveniently and quickly. Previously, the FEA has been employed to study the ballistic test of neat fabric [35–38]. Among them, Chen [39,40] and Nilakantan [30,41] et al. made a lot of inspiring work which demonstrated the failure mechanism of fabric. However, due to the mechanical difficulties, the ballistic simulation of STF/Kevlar was rare [42]. Lee [43] and Hasanzadeh [44] et al. conducted some meaningful investigations. It was found that the simulation result can be corresponded well to the experiment by adjusting the contact behavior between fabric yarns. However, most of the current simulations are only focused on qualitatively corresponding to the experiments, a more comprehensive comparison and interpretation of the experiment are still lacking. To better explore the mechanism of protection or material reinforcement, the numerical simulation on STF/Kevlar is necessary.

In this work, the C-STF/Kevlar composite was fabricated by a high performance CNT doped STF (C-STF). The effect of volume fraction of dispersed phase in STF, CNT addition content and fabric layers on the ballistic performance of composite were studied comprehensively. The quasi-static puncture and yarn pull-out experiments were employed to demonstrate the effect of STF on yarn friction. Combined with FEA, the impact process was simulated and analyzed, and the results in the experiment were well matched with the simulation. The reinforcement mechanism for STF on the Kevlar fabric was revealed, and this work provided guidance for the designation of high performance soft body armor.

2. Materials and methods

2.1. Preparation of STFs and composites

The PSt-EA nanoparticles which were prepared by soap free emulsion polymerization were chosen as the disperse phase. The CNT was firstly homogeneously dispersed in a solvent consist of ethyl alcohol and acetone and then dispersed into ethylene glycol (EG). After removing ethyl alcohol and acetone, the CNT/EG mixture was obtained. The STFs were fabricated by dispersing the PSt-EA nanoparticles into EG or CNT/EG mixtures. To investigate the effect of PSt-EA volume fraction and CNT weight fraction, five types of STF and C-STF were prepared.

In this research, the fabric was a kind of plain-woven aramid Kevlar fabric with an areal density of 200 g/m^2. To fabricate the Kevlar composites, the STFs samples were firstly diluted 1:2 with water and then mixed for 30 min in ultrasonication to ensure the solution well-distributed. The Kevlar fabric was cut into approximately 11.3 × 11.3 cm and impregnated in the solution individually for 5 min. After the impregnation, the fabric was dried at 55 °C for 10 min to evaporate the water. For simplicity, the definition and the specific parameters of the samples are shown in Table 1.

2.2. Methods

2.2.1. Rheological test

The rheological properties of STF and C-STF samples were tested by the rheometer (Anton-Paar MCR 301) with cone-plate geometry (25 mm in diameter and 2° in cone angle). All the experiments were conducted with a gap size of 0.05 mm at a room temperature of 25 °C. A pre-shear was used to provide consistent flow.

2.2.2. Ballistic impact test

In this research, a spherical bullet (diameter 8 mm) was driven by a gas gun. A couple of laser velocimeters were set on the muzzle to record the incident velocity of bullet. The fabric was securely fixed by the clamp by twelve screws and groove structure (Fig. 2a). The impact area was 85 × 85 mm. The target sample was fixed in close with the muzzle (15 cm) so that the yaw and velocity decay of projectile could be neglected. The high-speed video camera placed at the back of the impact sample was used to capture the deformation and destruction process of fabrics and record the projectile position for calculating its residual velocity.

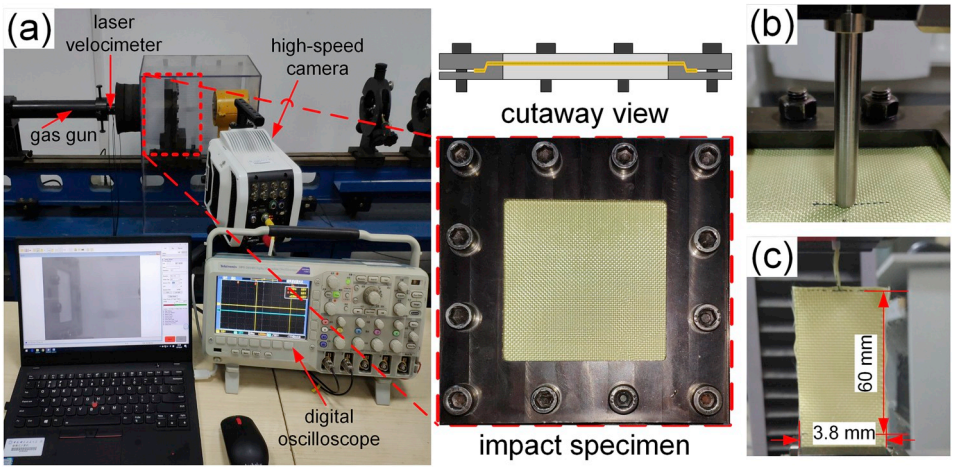

Fig. 1. The experimental configuration of (a) ballistic impact, (b) quasi-static puncture and (c) yarn pull-out test system.

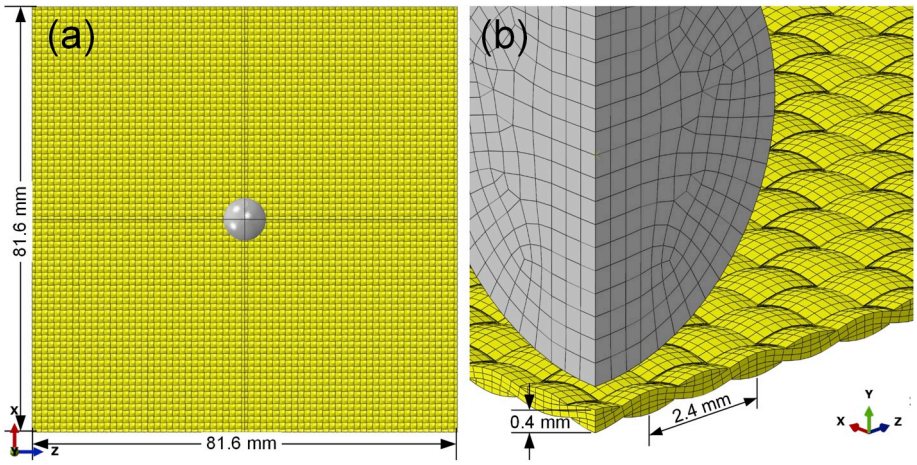

Fig. 2. (a) The initial geometrical configuration for a spherical projectile impacting on the center of Kevlar fabric. (b) Details of the quarter symmetric 3D finite element mesh of the initial geometry.

Table 2
The material parameters of Kevlar in Abaqus.

Parameter	Value
density	1.44e-9 tonne/mm^3
E_{11}	88000 MPa
E_{22}, E_{33}	2000 MPa
G_{12}, G_{13}, G_{23}	2000 MPa
ν_{12}, ν_{13}, ν_{23}	0.36
Fracture strain	0.036
Damage evolution energy	72 mJ
Yield stress at zero plastic strain	2000 MPa
Yield stress	3000 MPa
Plastic strain at yield stress	0.08

2.2.3. Quasi-static puncture test

A quasi-static puncture experiment was carried out on a universal tensile instrument (MTS Criterion™ Model 43) to study the evolution of the contact force of the fabric under vertical load. The rounded tip penetrator with a diameter of 8 mm and a length of 60 mm was clamped and was moved with a speed of 2 mm/min (Fig. 2b). The samples were clamped in the same fixture as in the ballistic impact experiment. The penetrator was pushed into the center of the sample and force-displacement diagrams were obtained for all samples.

2.2.4. Yarn pull-out test

To study the friction between yarns, the yarn pullout test was conducted the tensile instrument. As shown in Fig. 1c, the size of specimens was 38 mm × 60 mm. The tail of the pulled yarn was cut off and its head was clamped. The pull-out forces and displacement were recorded. In this experiment, the pull out speed varied from 2, 5, 20, 50–200 mm/min.

2.2.5. Finite element analysis (FEA)

In this research, the finite element (FE) model was created in Abaqus/Explicit. In order to save computing time, only a quarter of the system was modeled since the symmetry of impact system. Fig. 2a shows the initial geometry of the impact system: an 8.0 mm diameter rigid steel sphere with a density of 7.95 g/cm^3 impacting the center of an 81.6 × 81.6 mm square plain-woven fabric in the normal direction. The fabric model was created at the yarn cluster-level. For simplicity, the warp and weft yarns were the same in geometry and material property. The cross-section of the yarn was composed of two identical sine curves facing each other. The yarn path had a sinusoidal shape. The yarn thickness was 0.2 mm and the yarn crimp wavelength was 2.4 mm.

The steel sphere was defined as a kind of isotropic elastic material

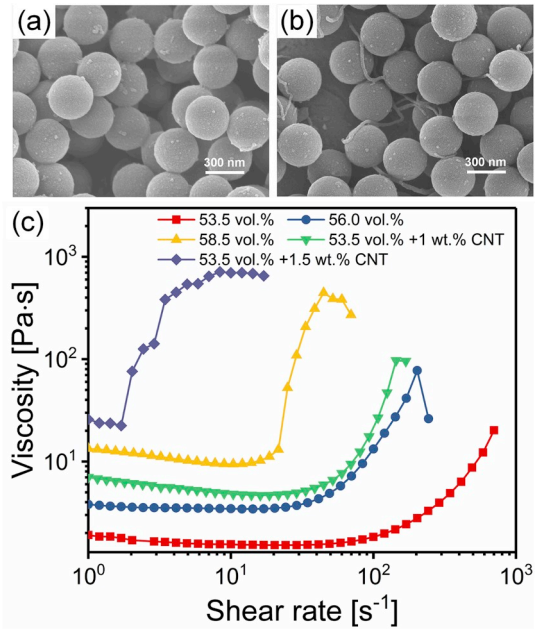

Fig. 3. SEM pictures of (a) PSt-EA and (b) PSt-EA and CNT. (c) Typical rheological curves of STFs.

with an elastic modulus of 200 GPa. Besides, it was also constrained by the rigid body and moved in a direction normal to the X-Z plane. The yarns were considered to be transversely isotropic material. The material constants were dominated by the longitudinal tensile modulus. From the result of yarn tensile test (for details, see Supplementary Information, Fig. S2), it can be inferred that $E_{11} = 88$ *GPa*. In most studies [35,36,45,46], the transverse elastic moduli (E_{22} and E_{33}) and shear moduli (G_{12}, G_{13}, and G_{23}) were assumed to be much smaller than E_{11}. Ductile damage was assigned to simulate the fabric breakage during impact [36]. The detailed parameters are shown in Table 2. All edges of Kevlar fabric were clamped in the simulation.

General contact (Explicit) was selected in the simulation. Yarn–yarn and projectile–fabric contact were generated using a hard contact-penalty algorithm provided by the Abaqus/Explicit. The friction coefficient of Kevlar fabric between yarns was 0.21 according to the experimental result (for details, see Supplementary Information, Table S1). Sweep meshes were generated in the yarns. The FE Kevlar fabric model involved 166464 C3D8R elements. Besides, the projectile

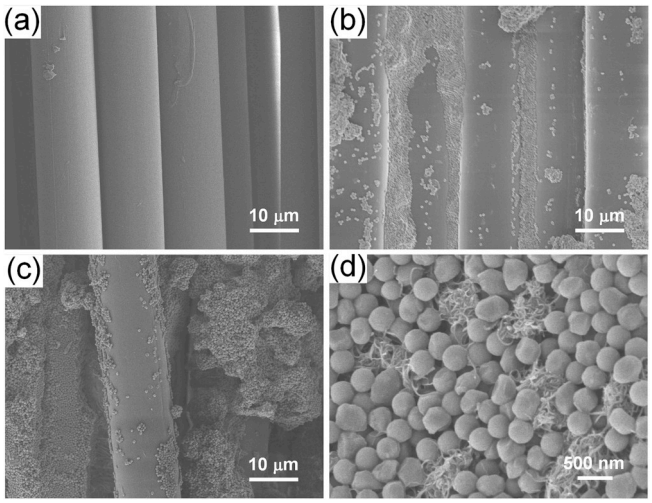

Fig. 4. SEM images of neat Kevlar and STF/Kevlar composites: (a) neat Kevlar fabric, (b) STF/Kevlar composite, (c) C-STF/Kevlar composite. (d) The distribution of CNT and PSt-EA nanoparticles on the surface of Kevlar.

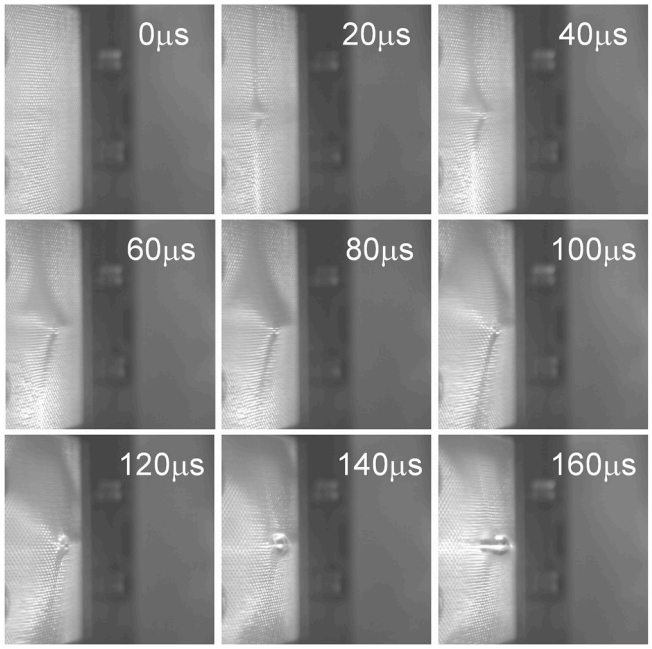

Fig. 5. Impact process of neat Kevlar at $v_i = 120$ m/s.

was meshed with 2928 C3D8R elements and 384 C3D6 elements.

3. Results and discussion

3.1. Characterization of STFs and composites

Fig. 3 shows the SEM figures of PSt-EA and CNT/PSt-EA. As can be seen from Fig. 3a and b, the PSt-EA particles are monodisperse with an average particle size of about 350 nm. After doping, the CNT and PSt-EA particles are well mixed and the CNT is uniformly distributed. Fig. 3c presents the typical viscosity curves of STF and C-STF. As the volume fraction of PSt-EA in STF increases from 53.5%, 56%, to 58.5%, the critical shear rate decreases from 35 s^{-1}, 21 s^{-1}, to 12 s^{-1}, the maximum viscosity increases from 20 Pa·s, 78 Pa·s to 446 Pa·s, respectively. The volume fraction of PSt-EA shows a great influence on the rheological behavior of STF. In comparison to single-phase STF, by doping the 1.0 wt % CNT, the C-STF (53.5 vol %) behaves the rheological property similar to the 56 vol % PSt-EA based STF. Besides, as the CNT content reaches to 1.5%, the critical shear rate of C-STF decreases to 1.7 s^{-1} and the maximum viscosity increases to 713 Pa·s. The presence of CNT prevents the movement of the PSt-EA particles, making the particles easier to be aggregated, so the shear thickening in C-STF is more likely to occur. The addition of CNT can significantly improve the shear thickening effect of STF.

Fig. 4 depicts the microstructure of the STF/Kevlar and C-STF/Kevlar composites. Compared with the neat Kevlar (Fig. 4a), the surfaces of STF/Kevlar composites are rougher. The STF is distributed over the surface of the fabric and filled the spaces between the fabric yarns (Fig. 4b). Fig. 4c and d shows that the addition of CNT can cause more STF to adhere to the surface of the fabric, but the particles in the STF will agglomerate on the surface of the fiber due to the presence of CNT.

3.2. Ballistic impact test

Fig. 5 depicts the impact process of neat Kevlar. The stress wave propagates in the yarns at a velocity of $v_s = \sqrt{E/\rho}$ and it propagates the entire fabric within 20 μs, where E is the tensile modulus along the yarn path and ρ is the yarn density. The fabric is initially damaged at 100 μs and the projectile completely penetrates the fabric at 160 μs. The residual velocity can be obtained using the position of projectile after penetration. The impact processes of STF/Kevlar and C-STF/Kevlar are similar with SN, except that the STFs will splash during impact.

To investigate the influence of volume fraction of STF on the ballistic resistance of STF/Kevlar, three types of composites were tested. Besides, SN and SE were tested as a comparison. Fig. 6a presents the residual velocities of samples at different incident velocities. If the test result is biased, the test was repeated several times. In particular, in order to obtain a more accurate ballistic limit speed, the repeated tests were performed several times. The relationship between residual velocity and incident velocity is fitted by the Recht-Ipson [47] function:

$$v_r = \alpha(v_i^p - v_{bl}^p)^{1/p} \tag{1}$$

where v_r and v_i are the residual velocity and incident velocity of projectile, α and p are the parameters controlling the shape of curve, v_{bl} is the ballistic limit velocity. The fitting results are shown in solid lines. It is clear that the function fits well to the experimental results. Taking SN for example, when the v_i is high enough, the v_r and v_i are approximately linear: $v_r \propto v_i$. However, as the v_i approaches v_{bl}, the v_r decreases sharply. When $v_i < v_{bl}$, the fabric cannot be penetrated and the v_r is considered to be 0. The v_{bl} of SE is 76.6 m/s, which is lower than the neat Kevlar's 84.6 m/s. The EG comparison group is only to illustrate that the dispersion medium EG in the STF does not enhance the ballistic resistance property of Kevlar. The STF/Kevlar composites have higher ballistic limit velocities compared with neat Kevlar. As the volume fraction of STF increases from 53.5% to 58.5%, the corresponding ballistic limit velocity increases from 92.9 m/s to 99.5 m/s. Fig. 6d depicts the dissipation energy of the samples in Fig. 6a. The dissipation energy is defined as:

$$E_{dis} = \frac{1}{2}mv_i^2 - \frac{1}{2}mv_r^2 \tag{2}$$

where m is the mass of projectile. The STF/Kevlar can dissipate more energy compared with neat Kevlar. The dissipated energy of the composite is positively correlated with the volume fraction of the STF. It can be concluded that by impregnating the high volume fraction STF, the ballistic resistance performance of Kevlar can be greatly enhanced.

The effect of CNT on the ballistic resistance property of C-STF/Kevlar is shown in Fig. 6b and e. Compared with SF1, the v_{bl} of SC1 increases from 92.9 m/s to 96.5 m/s. The addition of CNT can effectively improve the ballistic resistance property of STF/Kevlar. However, when the weight fraction of CNT increases to 1.5%, although the v_{bl} of SC2 is still

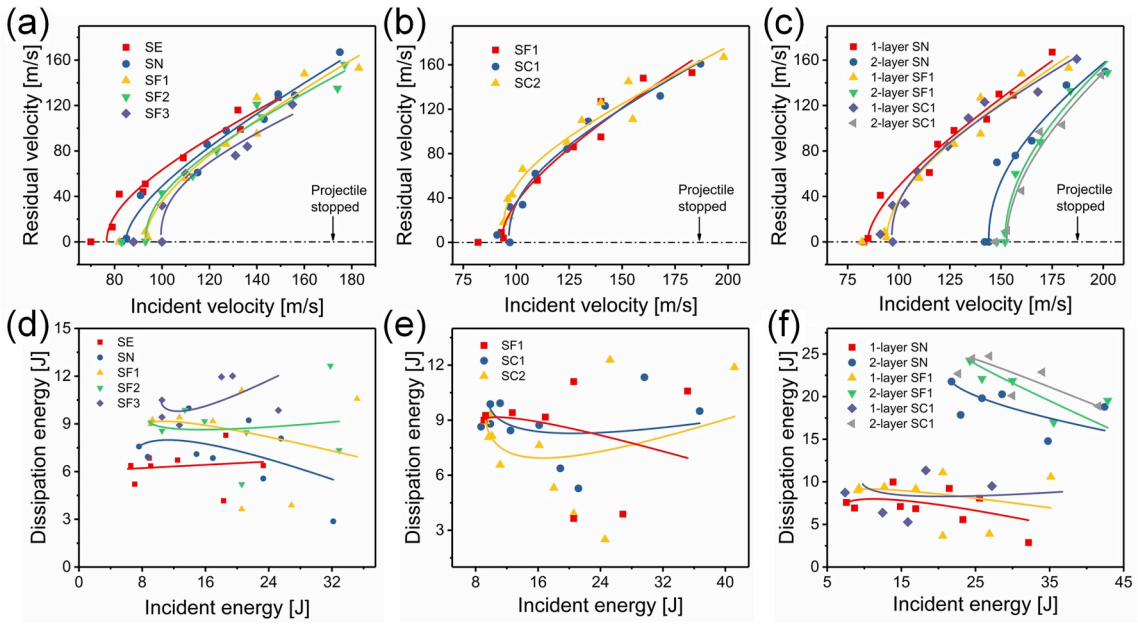

Fig. 6. The residual velocity results of (a) different volume fraction of STF, (b) different CNT concentrations and (c) different layers under varies incident velocities. The symbols are the experimental results and the solid lines are the Recht-Ipson fitting results. The (d), (e) and (f) are the corresponding energy dissipation results. The solid lines are calculated from the residual velocities obtained by the Recht-Ipson fitting.

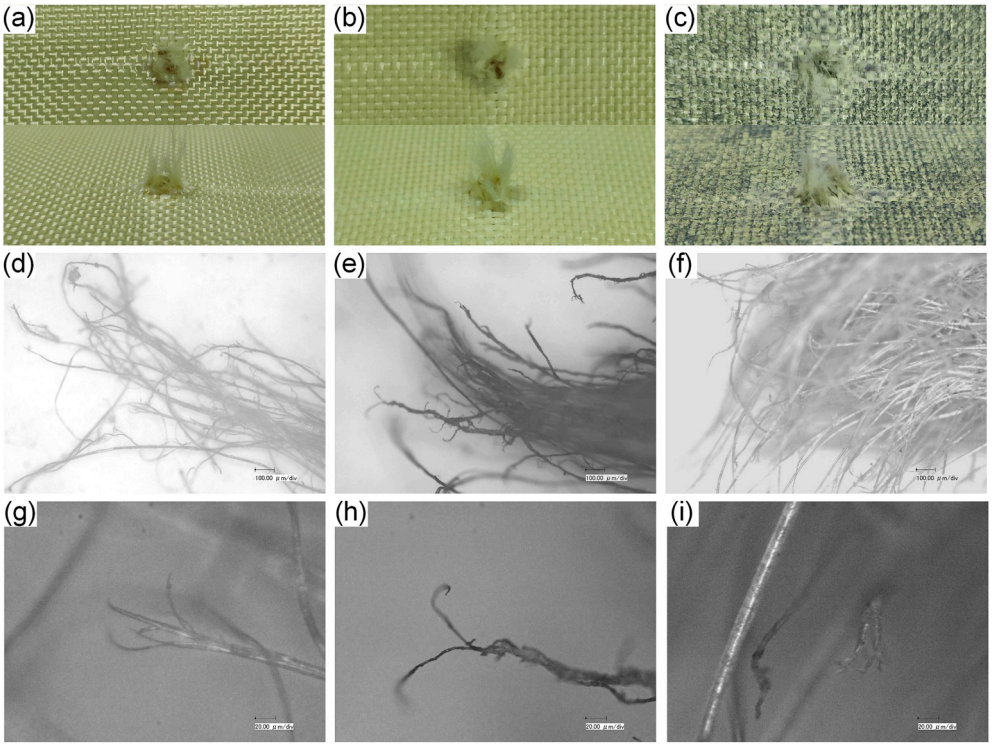

Fig. 7. The macroscopic features of (a) SN, (b) SF2 and (c) SC2 under the top and side view. (d), (e) and (f) are the microscopic features of fractured yarns corresponding to (a), (b) and (c). Besides, (g), (h) and (i) are the magnified details corresponding to (d), (e) and (f).

higher than that of SF1, it is significantly lower than that of SC1. Besides, the SC2 presents the worst energy dissipation result. When the concentration of CNT is high, the particles in Kevlar are agglomerated by excessive CNT, causing excessive STF to adhere to the fabric surface. This unevenness weaken the protective property of Kevlar under high-speed impact. This shows that adding CNT within a certain range can further improve the ballistic performance of the composite, but when the amount of CNT exceeds a certain value, the improvement result is lowered.

In practical applications, multi-layer Kevlar can meet high protection requirements. In this research, two layers of fabric were tested for bulletproof. From the residual velocity results in Fig. 6c, the v_{bl} of two-layer fabric is almost 1.6 times larger than that of single layer. The v_r exhibits a stronger nonlinearity in the region where the v_i is close to v_{bl}.

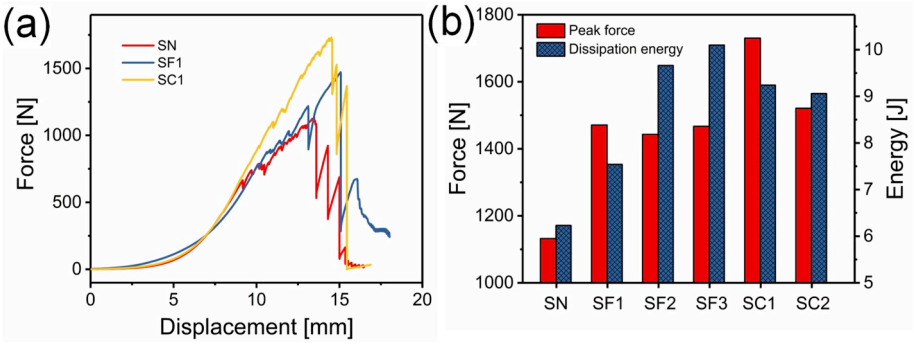

Fig. 8. (a) The puncture force curves of SN, SF1 and SC1. (b) Comparison of Peak puncture force and dissipation energy.

The ballistic resistance property of two-layer STF/Kevlar is still better than neat Kevlar. Adding CNT with a mass fraction of 1.0% (C-STF/Kevlar) can also enhance the protective property of two-layer STF/Kevlar. Fig. 6f depicts the energy dissipation of two-layer and single-layer samples. Two-layer fabric dissipates more energy than twice that of the single layer because of the interlayer friction.

To investigate the failure mode of fabric yarns during ballistic impact, the microscopic and macroscopic structures of Kevlar, STF/Kevlar, and C-STF/Kevlar fabrics were studied. Fig. 7a–c shows a similar character: The fractured yarns are obviously stretched and the length of the yarn heads in the fracture area are different. The C-STF on the surface of the SC2 near the impact region is splashed off due to the impact. During the ballistic impact, the filaments may be subject to two kinds of failure modes: the tensile failure and the shear failure. The failure mode of the fiber is determined by a lot of factors. Typically, the fracture surface of the fiber in the failure of the tensile failure is irregular, and the fiber fracture at the shear failure is flat. Fibers can dissipate more energy in the tensile failure mode [39]. Fig. 7d–i shows the microscopic features of fractured yarns of SN, SF2 and SC2. These figures depict a similar character: the filament breaks at different locations and the fiber breaks unevenly. The fractured sections of the yarns are not aligned, and the fractured yarns are bent or even bifurcated. This is quite different from the failure mode of fiber in the stab resistance test [4,24]. These results indicate that the fractured yarns of both the neat Kevlar and the composites are in tensile failure mode under a spherical projectile impact.

3.3. Quasi-static puncture test

The static puncture test was employed to investigate the change in the force of fabric during penetration. Although the strain rates of quasi-static and ballistic impacts vary widely, the contact force results in quasi-static conditions can give a qualitative explanation of the impact process. As shown in Fig. 8a, the puncture process can be divided into two stages: Firstly, the contact force rises slowly when the puncture displacement below around 6 mm. Then, the contact force increases rapidly with increasing displacement. In the first stage, the woven structure of the fabric is straightened, and in the second stage, the fabric yarns are stretched. The difference in the force-bearing structure of the fabric results in a change in the contact force. Compared with the neat Kevlar, the STF/Kevlar has a greater penetration force and the C-STF/

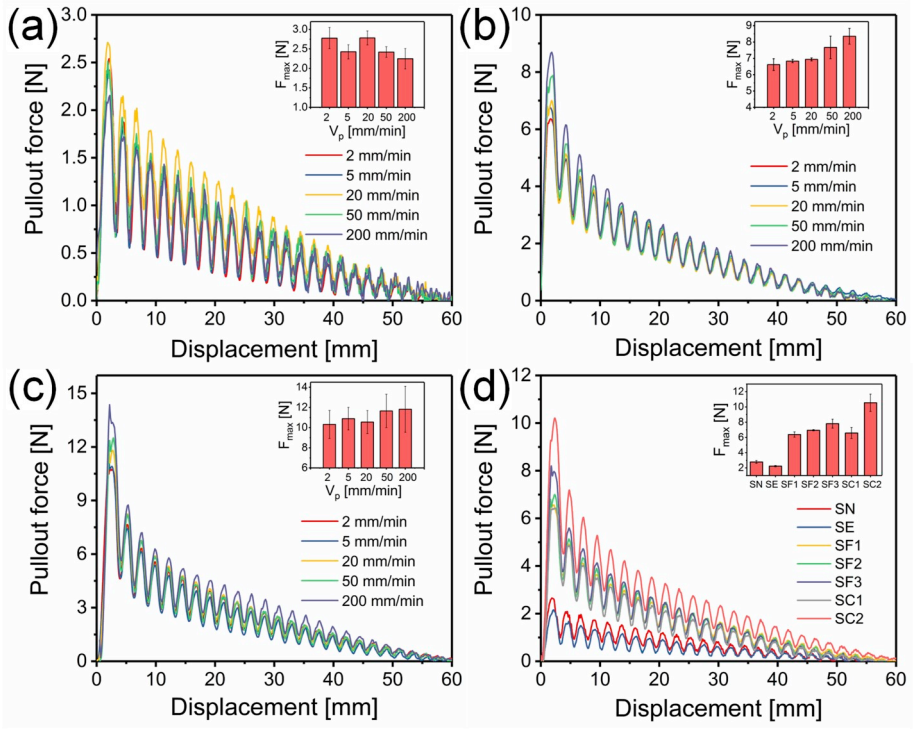

Fig. 9. Pull-out force versus displacement at different pull-out speeds for (a) neat Kevlar, (b) SF2 and (c) SC2. (d) The pull-out forces for different samples at a pull out speed of 20 mm/min.

Table 3
Friction coefficient of different samples.

Sample	μ
SN	0.21
SF1	0.48
SF2	0.52
SF3	0.59
SC1	0.50
SC2	0.80

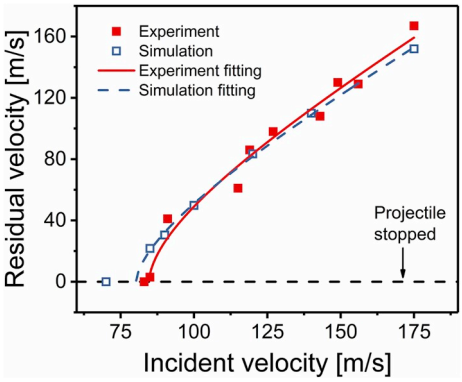

Fig. 10. Comparison of the residual velocity results between experiment and simulation of neat Kevlar.

Kevlar's puncture resistance is best. Fig. 8b shows the results of peak puncture force and dissipation energy for all samples. The impregnation of STF can enhance the puncture resistance of Kevlar. Besides, as the volume fraction of STF increases, the increase in peak puncture force is not obvious, while the dissipation energy increases significantly. The addition of CNT has an optimal weight fraction. The performance of SC1 is better than SC2.

3.4. Yarn pull-out test

When the fabric is subjected to load, the slip of yarn has an important influence on the mechanical properties of the fabric. The yarn pull-out test was carried out to investigate the friction between fabric yarns [46]. Fig. 9a depicts the pull-out forces versus displacement of neat Kevlar at different pull-out speeds. For simplicity, the pull-out force is a function of friction coefficient and compressive force [44,48,49] $F = f(\mu, F_N)$. For fabrics of the same woven structure, the contact normal force F_N at which the yarn is pulled out is approximately considered to be constant. Thus it can be concluded that $F \propto \mu$. In Fig. 6a, when the pull-out speed increases from 2 to 200 mm/min, the peak pull-out force F_{max} fluctuates around 2.5 N and does not change much. Then it can be approximated that the μ of neat Kevlar is rate-independent and is a constant. For STF/Kevlar composite, the F_{max} is 3 times larger than the neat Kevlar (Fig. 9b). Although the F_{max} behaves a trend of rate-dependent, it does not change very much. For example, the F_{max} of SF2 increases from 6.6 N to 8.4 N as the pull-out speed increases from 2 mm/min to 200 mm/min. The increase of F_{max} is only 1.8 N, which is much lower than 6.6 N. So the μ of STF/Kevlar is still considered as a constant for simplicity. Fig. 9c shows pull-out force versus displacement at different pull-out speeds for C-STF/Kevlar. Keeping the pull-out speed at 20 mm/min, the pull-out force versus displacement curves for all samples are compared (Fig. 9d). It is obvious that the F_{max} increases with the increasing volume fraction of STF. The addition of C-STF can enhance the friction between yarns compared with STF/Kevlar. According to the results of F_{max}, the friction coefficient μ for different samples are summarized in Table 3.

3.5. FEA results

FEA can obtain detailed data during the impact process, which is a good complement to the experimental results. Fig. 10 shows the comparison of experiment and simulation results of neat Kevlar. The v_{bl} of the simulation is 80.3 m/s and the experimental fitting result is 84.6 m/s. The error is only 5% for v_{bl}. The residual velocity curve obtained by simulation is highly consistent with the experimental result. Besides, the deformation of the fabric is also in good agreement with the experimental results (for details, see Supplementary Information, Fig. S8). So the simulation can make a good complement and analysis of impact experiments.

Fig. 11 depicts the impact process of neat Kevlar (v_i=120 m/s). When the projectile touches the fabric, the stress wave propagates the yarns within several microseconds. The stress in yarns rises with the increasing time. The fabric deforms under impact and the transverse wave propagates at a velocity of approximately 480 m/s. The penetration occurred at t = 80 μs, which is a little later than the experiment. Then the fabric morphology fluctuated due to the reflection of surface waves. Since the simulation does not take into account the influence of the incident airflow, the fluctuation of the fabric is more obvious than the experiment.

By inputting the friction coefficient obtained by the yarn pull-out

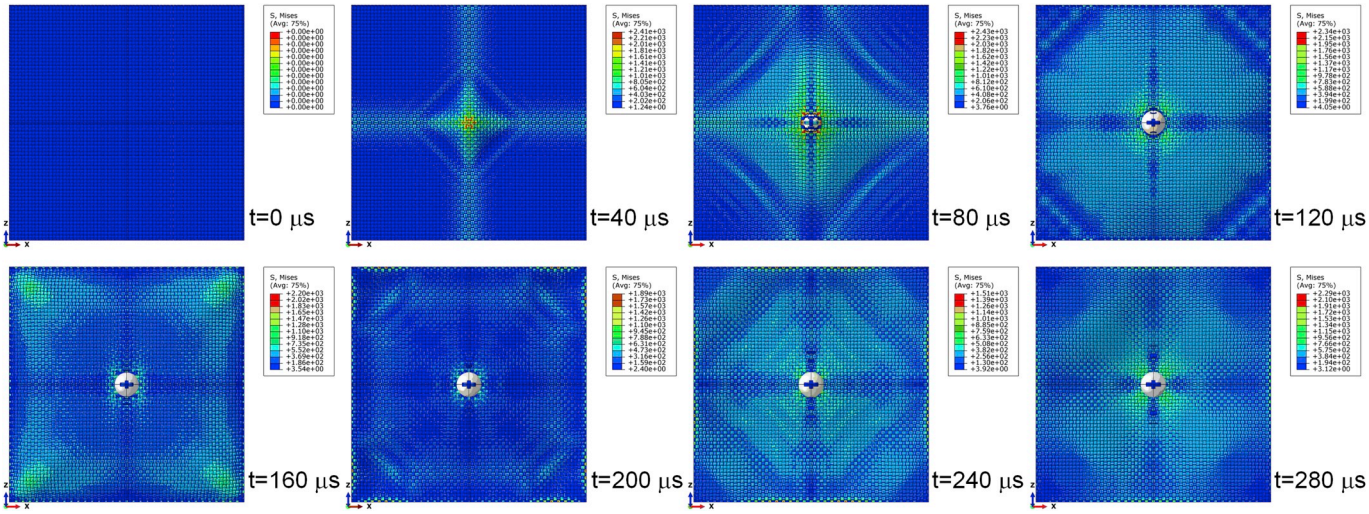

Fig. 11. Simulation results of stress distribution during impact (v_i=120 m/s).

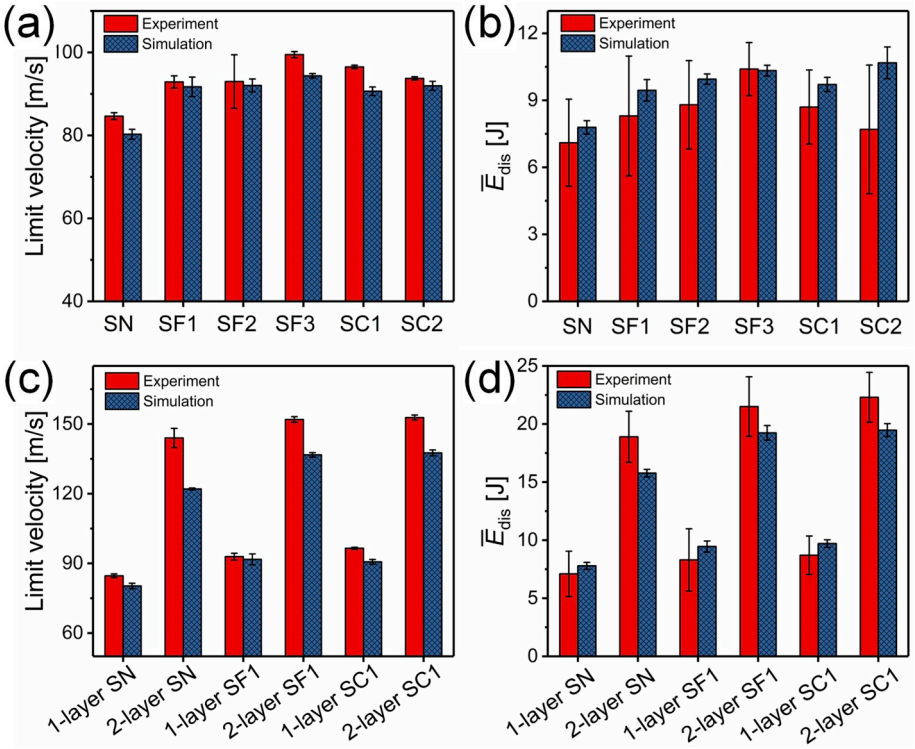

Fig. 12. The comparison of ballistic limit velocity and average dissipation energy ($\bar{E}_{dis}$) results obtained from experiments and simulations.

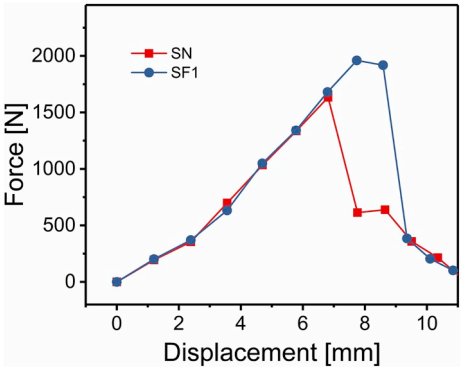

Fig. 13. Simulation results of contact force of SN and SF1 under projectile impact.

experiment into Abaqus/Explicit, the simulation results of STF/Kevlar and C-STF/Kevlar can be obtained. Fig. 12 gives the experimental and simulation results of the ballistic limit velocity and average dissipation energy. In general, the simulation and experimental results correspond well. The addition of STF or C-STF can increase the friction between the fabric yarns and thus more energy is dissipated under the impact (Fig. 12b). Finally, the v_{bl} (Fig. 12a) is increased and the ballistic performance of Kevlar is improved.

However, when the CNT is certain exceeded than the optimum, excessive C-STF on the surface of the fabric results in the non-uniformity in the fabric, and reduces the C-STF enhancement effect. In the simulation, since the unevenness of the fabric surface is not considered, the simulation and experimental results of SC2 are quite different. Two-layer STF/Kevlar and C-STF/Kevlar still show enhanced effects. But the effect of CNT is not obvious, whether it is from the v_{bl} or $\bar{E}_{dis}$ (Fig. 12c and d). In the experiment, the two layers of fabric dissipates more than twice the energy of a layer of fabric, while the simulation results show that the energy dissipated by the two layers of fabric is roughly equal to twice the energy dissipated by the layer of fabric. On the one hand, the two-layer fabric shows slight slippage during the experiment. On the other hand, the broken yarns in the simulation cannot bear the load.

As mentioned above, increasing friction can improve the ballistic performance of Kevlar. However, its specific mechanism of action is still unclear. Previous studies [12,19] have indicated that increasing friction can increase the load bearing area of the fabric. But this inference lacks verification. To this end, we studied the effect of friction coefficient on the force and deformation of the fabric through simulation. The simulation results show that increasing the friction can increase the bearing area of the fabric, and the stress of the fabric in the deformed area is more uniform. So the fabric can withstand higher impact (Fig. 13). The simulation results give a good explanation for the increment of the friction coefficient to the improvement of Kevlar's protection performance and correspond well to the previous conclusions.

4. Conclusion

In this paper, the ballistic performance of the composite is improved by adjusting the volume fraction of the particles in the STF and the amount of CNT addition. The results show that increasing the particle volume fraction of STF can enhance the ballistic performance of STF/Kevlar. The addition of CNT has an optimal value, and the protective effect of C-STF/Kevlar with CNT with a mass fraction of 1% is even better than 1.5%. The trend of the puncture force in the quasi-static puncture is roughly the same as the ballistic test result. The yarn pull-out results show that the STF can increase the friction between the yarns, and the addition of CNT further increases the pull-out force. The FEA results of ballistic impact are consistent with the experiment, and the influence of the increased friction coefficient of STFs on the ballistic limit velocity and dissipated energy is quantitatively analyzed. The simulation results directly show that the STFs increase the friction coefficient between the yarns, increase the bearing area of the fabric, and make the stress distribution more uniform, thereby improve the ballistic performance of Kevlar.

CRediT authorship contribution statement

Saisai Cao: Data curation, Formal analysis, Software, Visualization, Writing - original draft, Writing - review & editing. **Haoming Pang:** Investigation, Methodology. **Chunyu Zhao:** Formal analysis, Validation. **Shouhu Xuan:** Resources, Funding acquisition, Writing - review & editing. **Xinglong Gong:** Conceptualization, Supervision, Project administration, Resources, Funding acquisition, Writing - review & editing.

Acknowledgments

Financial supports from the National Natural Science Foundation of China (Grant No. 11772320, 11822209, 11972032), the Fundamental Research Funds for the Central Universities (WK2090050045), and the Strategic Priority Research Program of the Chinese Academy of Sciences (Grant No. XDB22040502) are gratefully acknowledged. This work was supported by Collaborative Innovation Center of Suzhou Nano Science and Technology.

Appendix A. Supplementary data

Supplementary data to this article can be found online at https://doi.org/10.1016/j.compositesb.2020.107793.

References

[1] Gurgen S, Kushan MC, Li W. Shear thickening fluids in protective applications: a review. Prog Polym Sci 2017;75:48–72.
[2] Bilisik K. Two-dimensional (2D) fabrics and three-dimensional (3D) preforms for ballistic and stabbing protection: a review. Textil Res J 2017;87(18):2275–304.
[3] Lin M, Lou C, Lin J, Lin T, Lin J. Mechanical property evaluations of flexible laminated composites reinforced by high-performance Kevlar filaments: tensile strength, peel load, and static puncture resistance. Compos B Eng 2019;166:139–47.
[4] Gong X, Xu Y, Zhu W, Xuan S, Jiang W, Jiang W. Study of the knife stab and puncture-resistant performance for shear thickening fluid enhanced fabric. J Compos Mater 2014;48(6):641–57.
[5] Gurgen S. Wear performance of UHMWPE based composites including nano-sized fumed silica. Compos B Eng 2019;173:106967.
[6] Brown E, Jaeger HM. Shear thickening in concentrated suspensions: phenomenology, mechanisms and relations to jamming. Rep Prog Phys 2014;77(4):046602.
[7] Barnes HA. Shear-thickening (Dilatancy) in suspensions of nonaggregating solid particles dispersed in Newtonian liquids. J Rheol 1989;33(2):329–66.
[8] Mawkhlieng U, Majumdar A. Deconstructing the role of shear thickening fluid in enhancing the impact resistance of high-performance fabrics. Compos B Eng 2019;175:107167.
[9] Gurgen S, Sert A. Polishing operation of a steel bar in a shear thickening fluid medium. Compos B Eng 2019;175:107127.
[10] Fu K, Wang H, Chang L, Foley M, Friedrich K, Ye L. Low-velocity impact behaviour of a shear thickening fluid (STF) and STF-filled sandwich composite panels. Compos Sci Technol 2018;165:74–83.
[11] Spinelli DJ, Plaisted TA, Wetzel ED. Adaptive head impact protection via a rate-activated helmet suspension. Mater Des 2018;154:153–69.
[12] Zhao Q, He Y, Yao H, Wen B. Dynamic performance and mechanical model analysis of a shear thickening fluid damper. Smart Mater Struct 2018;27(7):075021.
[13] Peng H, Wang D, Li M, Zhang L, Liu M, Fu S. Ultra-small SiO_2 nanospheres self-pollinated on flower-like MoS_2 for simultaneously reinforcing mechanical, thermal and flame-retardant properties of polyacrylonitrile fiber. Compos B Eng 2019;174:107037.
[14] Jiang W, Sun Y, Xu Y, Peng C, Gong X, Zhang Z. Shear-thickening behavior of polymethylmethacrylate particles suspensions in glycerine-water mixtures. Rheol Acta 2010;49(11–12):1157–63.
[15] Zhang H, Zhang X, Chen Q, Li X, Wang P, Yang E-H, et al. Encapsulation of shear thickening fluid as an easy to-apply impact-resistant material. J Mater Chem 2017;5(43):22472–9.
[16] Cao S, He Q, Pang H, Chen K, Jiang W, Gong X. Stress relaxation in the transition from shear thinning to shear jamming in shear thickening fluid. Smart Mater Struct 2018;27(8):085013.
[17] Fu K, Wang H, Wang S, Chang L, Shen L, Ye L. Compressive behaviour of shear-thickening fluid with concentrated polymers at high strain rates. Mater Des 2018;140:295–306.
[18] Lee YS, Wetzel ED, Wagner NJ. The ballistic impact characteristics of Kevlar (R) woven fabrics impregnated with a colloidal shear thickening fluid. J Mater Sci 2003;38(13):2825–33.
[19] Haro EE, Szpunar JA, Odeshi AG. Ballistic impact response of laminated hybrid materials made of 5086-H32 aluminum alloy, epoxy and Kevlar (R) fabrics impregnated with shear thickening fluid. Compos Part A Appl S 2016;87:54–65.
[20] He Q, Cao S, Wang Y, Xuan S, Wang P, Gong X. Impact resistance of shear thickening fluid/Kevlar composite treated with shear-stiffening gel. Compos Part A Appl S 2018;106:82–90.
[21] Na W, Ahn H, Han S, Harrison P, Park JK, Jeong E, et al. Shear behavior of a shear thickening fluid-impregnated aramid fabrics at high shear rate. Compos B Eng 2016;97:162–75.
[22] Cao S, Chen Q, Wang Y, Xuan S, Jiang W, Gong X. High strain-rate dynamic mechanical properties of Kevlar fabrics impregnated with shear thickening fluid. Compos Part A Appl S 2017;100:161–9.
[23] Asija N, Chouhan H, Gebremeskel SA, Singh RK, Bhatnagar N. High strain rate behavior of STF-treated UHMWPE composites. Int J Impact Eng 2017;110:359–64.
[24] Decker MJ, Halbach CJ, Nam CH, Wagner NJ, Wetzel ED. Stab resistance of shear thickening fluid (STF)-treated fabrics. Compos Sci Technol 2007;67(3–4):565–78.
[25] Xu Y, Chen X, Wang Y, Yuan Z. Stabbing resistance of body armour panels impregnated with shear thickening fluid. Compos Struct 2017;163:465–73.
[26] Li W, Xiong D, Zhao X, Sun L, Liu J. Dynamic stab resistance of ultra-high molecular weight polyethylene fabric impregnated with shear thickening fluid. Mater Des 2016;102:162–7.
[27] Park Y, Kim Y, Baluch AH, Kim C-G. Empirical study of the high velocity impact energy absorption characteristics of shear thickening fluid (STF) impregnated Kevlar fabric. Int J Impact Eng 2014;72:67–74.
[28] Tan Z, Li W, Huang W. The effect of graphene on the yarn pull-out force and ballistic performance of Kevlar fabrics impregnated with shear thickening fluids. Smart Mater Struct 2018;27(7):075048.
[29] Khodadadi A, Liaghat G, Vahid S, Sabet AR, Hadavinia H. Ballistic performance of Kevlar fabric impregnated with nanosilica/PEG shear thickening fluid. Compos B Eng 2019;162:643–52.
[30] Nilakantan G, Merrill RL, Keefe M, Gillespie JW, Wetzel ED. Experimental investigation of the role of frictional yarn pull-out and windowing on the probabilistic impact response of kevlar fabrics. Compos B Eng 2015;68:215–29.
[31] Hasanzadeh M, Mottaghitalab V, Babaei H, Rezaei M. The influence of carbon nanotubes on quasi-static puncture resistance and yarn pull-out behavior of shear-thickening fluids (STFs) impregnated woven fabrics. Compos Part A Appl S 2016;88:263–71.
[32] Mittal G, Nešović K, Rhee KY, Mišković-Stanković V. Investigation of corrosion behaviour of carbon nanotubes coated basalt fabric as a reinforcement material. Compos B Eng 2019;178:107493.
[33] Gurgen S, Kushan MC. The ballistic performance of aramid based fabrics impregnated with multi-phase shear thickening fluids. Polym Test 2017;64:296–306.
[34] Yadav BN, Muchhala D, Singh P, Venkat ANC, Mondal DP. Synergic effect of MWCNTs and SiC addition on microstructure and mechanical properties of closed-cell Al-SiC-MWCNTs HCFs. Compos B Eng 2019;172:458–71.
[35] Duan Y, Keefe M, Bogetti TA, Cheeseman BA. Modeling friction effects on the ballistic impact behavior of a single-ply high-strength fabric. Int J Impact Eng 2005;31(8):996–1012.
[36] Rao MP, Duan Y, Keefe M, Powers BM, Bogetti TA. Modeling the effects of yarn material properties and friction on the ballistic impact of a plain-weave fabric. Compos Struct 2009;89(4):556–66.
[37] Parsons EM, King MJ, Socrate S. Modeling yarn slip in woven fabric at the continuum level: simulations of ballistic impact. J Mech Phys Solid 2013;61(1):265–92.
[38] Sun D, Chen X, Lewis E, Wells G. Finite element simulation of projectile perforation through a ballistic fabric. Textil Res J 2013;83(14):1489–99.
[39] Chen X, Zhu F, Wells G. An analytical model for ballistic impact on textile based body armour. Compos B Eng 2013;45(1):1508–14.
[40] Chu Y, Min S, Chen X. Numerical study of inter-yarn friction on the failure of fabrics upon ballistic impacts. Mater Des 2017;115:299–316.
[41] Nilakantan G, Keefe M, Bogetti TA, Adkinson R, Gillespie JW. On the finite element analysis of woven fabric impact using multiscale modeling techniques. Int J Solid Struct 2010;47(17):2300–15.
[42] Park Y, Kim Y, Baluch AH, Kim C-G. Numerical simulation and empirical comparison of the high velocity impact of STF impregnated Kevlar fabric using friction effects. Compos Struct 2015;125:520–9.
[43] Lee BW, Kim CG. Computational analysis of shear thickening fluid impregnated fabrics subjected to ballistic impacts. Adv Compos Mater 2012;21(2):177–92.
[44] Hasanzadeh M, Mottaghitalab V, Rezaei M, Babaei H. Numerical and experimental investigations into the response of STF-treated fabric composites undergoing ballistic impact. Thin-Walled Struct 2017;119:700–6.
[45] Zhu D, Soranakom C, Mobasher B, Rajan SD. Experimental study and modeling of single yarn pull-out behavior of kevlar® 49 fabric. Compos Part A Appl S 2011;42(7):868–79.
[46] Tapie E, Guo YB, Shim VPW. Yarn mobility in woven fabrics - a computational and experimental study. Int J Solid Struct 2016;80:212–26.
[47] Recht RF, Ipson TW. Ballistic perforation dynamics. J Appl Mech 1963;30(3):384–90.
[48] Badrossamay MR, Hosseini Ravandi SA, Morshed M. Fundamental parameters affecting yarn-pullout behavior. J Text Inst 2001;92(3):280–7.
[49] Bai R, Ma Y, Lei Z, Feng Y, Liu C. Energy analysis of fabric impregnated by shear thickening fluid in yarn pullout test. Compos B Eng 2019;174:106901.